16th World Congress in Computational Mechanics (WCCM)
21-26 July 2024, Vancouver, Canada
A. Korobenko, M. Laforest, S. Prudhomme, R. Vaziri (Eds)

UNDERSTANDING THE SOLIDIFICATION AND HEAT TREATMENT CHARACTERISTICS IN THE $CoCrNiSi_x$ MEDIUM-ENTROPY ALLOY BY EXPERIMENTALLY VERIFIABLE MULTISCALE THERMODYNAMIC AND KINETIC COMPUTATIONAL TECHNIQUES

H.C. HUANG[1], J.S. CHEN[1], J.J. CHEN[1], K.F. LIN[1], H.C. LIN[1], J.R. YANG[1] AND T.C. SU[1*]

[1] Department of Materials Science and Engineering, National Taiwan University
No. 1, Sec. 4, Roosevelt Road, Taipei, 10617 Taiwan(R.O.C.)
f11527060@ntu.edu.tw; johnchen@ntu.edu.tw; f08527053@ntu.edu.tw; kafainlin@gmail.com; hclinntu@ntu.edu.tw; jryang@ntu.edu.tw; *tcterrysu@ntu.edu.tw (*corresponding author)

Key words: Medium-Entropy Alloy (MEA), Solidification Microstructure, CALPHAD, FEM, Heat Transfer Model, Mesoscale Phase-Field Simulation.

Abstract. CoCrNi medium-entropy alloy (MEA) possesses an FCC crystal structure with multiple slip systems and low stacking fault energy [1]; a substantial amount of nanoscale deformation twins can be generated under low-temperature and high-speed deformation. Adding a proper amount of Si can not only reduce the manufacturing cost and mass density but also enhance ballistic resistance by further lowering the stacking fault energy. Previous studies [2] utilized small-scale vacuum arc remelting techniques to investigate the solid solution or secondary phase strengthening of CoCrNi-based MEAs with Al or Si additions. However, to extend the application of lightweight, high-entropy alloys to industrial-grade impact-resistant plate manufacturing, especially for low-temperature environments, it is necessary to study the solidification and heat treatment characteristics of $CoCrNiSi_x$ castings. This study employs finite element analysis at the macroscopic scale to investigate the solidification phase transformation and heat transfer characteristics of $CoCrNiSi_x$ under precision-cast conditions. Additionally, at the mesoscopic scale, the phase-field method [3] is used to simulate the dendritic solidification microstructure and element segregation of $CoCrNiSi_x$. Thermodynamic parameters required for simulations are calculated using Thermo-Calc high-entropy alloy databases TCHEA6 and MOBHEA2. This research also utilizes electron microscopy to analyze the microstructures of chemically complex $CoCrNiSi_x$ ingots, focusing on measuring the secondary dendrite arm spacing and elemental segregation profiles. Collecting these microstructure-related features allows us to reasonably infer the cooling rate corresponding to the investment casting process of $CoCrNiSi_x$ and design rational parameter combinations for homogenization heat treatment of the cast ingots in terms of temperature and isothermal holding time. By validating macroscopic and mesoscopic simulation results through $CoCrNiSi_x$ microstructure analysis experiments, the multiscale kinetic computational techniques included in this study can be further applied to cost-saving and process optimization practices in the manufacturing of various lightweight high-entropy alloys.

1 INTRODUCTION

Medium-entropy alloys (MEAs) are a novel class of multicomponent alloys containing 3-4 principal elements with a mixing entropy between $1\sim1.5R$ (R is the gas constant). The design principles for MEAs are similar to those for high-entropy alloys (HEAs), and they can exhibit the four core effects of HEAs [4-6]. MEAs also perform excellent mechanical properties. Compared to traditional Cantor Alloy CoCrFeMnNi, CoCrNi MEAs without Fe and Mn are more prone to generating nanoscale deformation twins under low temperatures and high strain rates, leading to significant enhancements in low-temperature strength, ductility, and fracture toughness [7]. In addition, adding lightweight elements can reduce the overall manufacturing melting cost and density and effectively improve the yield strength of FCC CoCrNi MEAs through solid solution strengthening and second-phase strengthening [2, 8-11].

However, most studies have only utilized small-scale vacuum arc remelting techniques, and research on CoCrNi MEA ingots manufactured through industrial casting processes is relatively scarce. The process parameters of ingot solidification, heat treatment, and the resulting microstructure have significant implications for subsequent plastic processing and mechanical properties. Theoretical considerations and numerous studies indicated that the secondary dendrite arm spacing (SDAS) and the grain size would decrease with increasing temperature gradients, cooling rates, or solidification undercooling under casting conditions [12-17]. Zheng et al. [18] further investigated the impact of SDAS on mechanical properties, confirming that grain refinement significantly enhances the strength of Cantor Alloy. Moreover, in ingot structures, the distribution of solute atoms and their transport phenomena play a crucial role in grain growth and solidification segregation [19, 20]. According to Liu's research [21, 22], adding C in CoCrNi or CoCrFeNi MEAs, besides serving as a lightweight element, also acts as a solute atom to promote constitutional supercooling. This behavior suppresses the growth of the columnar zone, promotes the transformation of columnar crystals into equiaxed dendrites during solidification, and further achieves grain refinement and reduces solidification segregation. Still, subsequent homogenization heat treatment on the as-cast ingot is required to eliminate solidification segregation and bring the ingot closer to thermodynamic equilibrium at the homogenization temperature. The thermal stability, ductility, and toughness of HEA or MEA ingots can be enhanced with proper process parameters.

Numerical simulation is a highly efficient and economically viable method to understand better the impact of process parameters on heat-transfer characteristics and the microstructure of castings. A range of scholars employed macroscale finite-element analysis to investigate the behavior of heat transfer, flow, and thermal stress during investment casting [23-26], a high-precision shape-casting variant. Additionally, numerous studies utilize phase field models to predict the microstructure of alloys and solve phase, heat, and solute transfer equations to describe microstructure evolution during solidification at the mesoscale. For example, Loginova et al. [27] analyzed the influence of spatial domain size and cooling rate on dendritic growth under non-isothermal solidification using the phase-field method. Kobayashi et al. [28] captured the differences between the isotropic and anisotropic growth of dendrites by incorporating variables related to material anisotropy. Beyond the solidification behavior of primary crystals, phase-field simulation methods are applicable for predicting grain and second-phase growth [29] and homogenization heat treatment processes to eliminate segregation [30].

It is evident that a comprehensive approach, combining multiscale experiments and

simulation methods, is crucial to explore the correlation among the process parameters, microstructure, and properties of industrial-grade MEA/HEA ingots. The experimental side of this study mainly utilized electron microscopy to directly observe the microstructure of $CoCrNiSi_x$ (x = 0.15 or 0.3) MEA ingots manufactured by investment casting, including the SDAS and interdendritic segregation behavior. A macroscale digital twin for investment casting was then developed by finite element analysis in order to investigate the solidification and heat transfer behavior of $CoCrNiSi_x$ MEA ingots. Additionally, we employed the phase-field method [3] to simulate the growth of dendrites and the segregation behavior at the mesoscale in $CoCrNiSi_x$ MEAs. Thermodynamic and kinetic parameters for simulation implementation were obtained using the calculation of phase diagrams (CALPHAD) method. Comparison of the analysis results with simulation outcomes not only allows for the reasonable inference of the solidification cooling rate during ceramic mold investment casting but also facilitates the optimization of parameters for homogenization heat treatment.

2 RESEARCH METHODS

2.1 Specimen preparation and microstructure analysis

$CoCrNiSi_{0.3}$ and $CoCrNiSi_{0.15}$ MEA ingots were prepared by vacuum induction melting (VIM), followed by ceramic mold investment casting. Before pouring liquid alloys, the mold was preheated to 1100°C. As-cast specimens would undergo 1, 3, 5, 10, 15, 20, 25, and 48 hours of homogenization heat treatments at 1100°C to eliminate the segregation. Specimens were ground with SiC papers and polished with Al_2O_3 suspension for microstructure characterization.

A field-emission electron probe microanalyzer (EPMA, JEOL JXA-8530F PLUS FE-EPMA) with wavelength dispersive spectrometer (WDS) was used to observe the element distribution and quantitatively analyze the component. The SDAS was measured using the image analysis software Fiji ImageJ.

2.2 CALPHAD analysis

The calculation of phase diagrams (CALPHAD) method was utilized to evaluate the solidification path and temperature-dependent thermodynamic parameters of $CoCrNiSi_x$ MEAs using Thermo-Calc with high-entropy alloy databases TCHEA7. Besides, the MOBHEA2 database for the DICTRA module in Thermo-Calc was also used to predict the solute transfer during the homogenization heat treatment. These evaluation outcomes were imported into the simulation models or compared to the experimental results.

2.3 Macroscale heat transfer modeling

The investment casting condition was simplified into a transient 2D finite element model in COMSOL Multiphysics® 6.1 to explore how the heat was extracted during the casting process. Fig. 1(a) shows the geometry of the whole heat transfer model, containing a 9cm x 9cm $CoCrNiSi_x$ MEA and a 4mm-thick ceramic mold. The scan line was used to visualize the results, which vary with time. The initial temperature of the $CoCrNiSi_x$ MEA and the preheated ceramic mold were set to be 1500°C and 1100°C, with the ambient temperature equal to 27°C. The surface emissivity of $CoCrNiSi_x$ MEA was assumed to be 0.15, and the thermodynamic parameters of the ceramic mold were assumed to be constants.

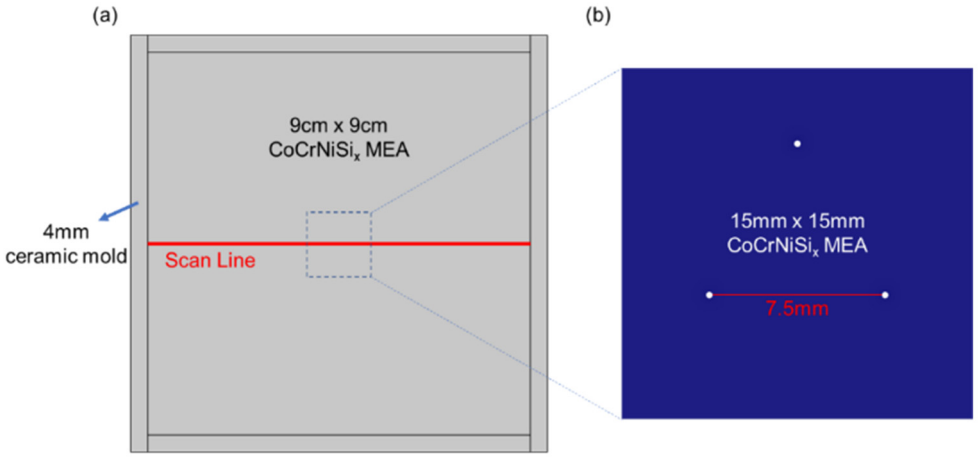

Figure 1. The geometry of (a) macroscale heat transfer model and (b) mesoscale phase field model (white dot indicates the nucleation points).

The general transient heat transfer formula can be obtained within COMSOL Multiphysics. However, in the current study, the convection in the liquid and the thermoelastic damping were not considered, so these two terms were neglected. Therefore, the partial differential equation for heat transfer control can be rewritten as:

$$d_z \rho C_p \frac{\partial T}{\partial t} + \nabla \cdot \boldsymbol{q} = q_0 \tag{1}$$

and

$$\boldsymbol{q} = -d_z k \nabla T \tag{2}$$

where d_z is the unit thickness, ρ is the density, C_p is the specific heat capacity, T is the temperature, t is the time, $\boldsymbol{q}$ is the conductive heat flux, k is the thermal conductivity, and q_0 is the inward heat flux.

The apparent heat capacity method was used to describe the phase transformation of the CoCrNiSi$_x$ MEAs solidified in the ceramic mold, and the specific heat capacity of the semi-solid MEA would vary with the solid fraction:

$$C_p = \theta_1 C_{p,1} + \theta_2 C_{p,2} + L_{1\to 2} \frac{\partial \alpha_m}{\partial T} \tag{3}$$

where θ_1 is the solid mass fraction, θ_2 is the liquid mass fraction, $L_{1\to 2}$ is the latent heat and α_m is the mass fraction.

The thermal contact model in the COMSOL heat transfer module was used to describe the heat transfer between the interfaces of the alloy and ceramic mold, and the equations can be written as [31]:

$$-\boldsymbol{n}_{\text{alloy}} \cdot \boldsymbol{q}_{\text{alloy}} = -h\left(T_{\text{mold}} - T_{\text{alloy}}\right) \tag{4}$$

$$-\boldsymbol{n}_{mold} \cdot \boldsymbol{q}_{mold} = -h\left(T_{alloy} - T_{mold}\right) \tag{5}$$

where $\boldsymbol{n}$ is the normal vector, $\boldsymbol{q}$ is the heat flux depends on the thermal conductivity and temperature difference in each material, and h is the heat transfer coefficient of the interfaces.

Finally, consider the heat loss by radiation from the ceramic mold surface to the environment:

$$-\boldsymbol{n}\cdot\boldsymbol{q} = d_z\varepsilon\sigma(T_{amb}^4 - T^4) \tag{6}$$

where ε is the surface emissivity assumed to be a constant 0.8, σ is the Stefan-Boltzmann constant, and T_{amb} is the ambient temperature equal to 27°C.

2.4 Mesoscale phase-field modeling

The microstructure evolution during solidification was predicted using a phase field model in MICRESS® (version 7.2). The simulated area was set at the center of the ingot with the size of 15mm x 15mm, as shown in Fig. 1(b). White spots spaced 7.5mm apart represent the locations of the nuclei. Temperature change in the area was obtained from COMSOL and was assumed to be uniform (i.e., no temperature gradients) and varying with time. FCC solid phase and liquid phase were the only two phases considered in the current model. The formulations of the phase field model in MICRESS were explained in detail in the literature [32-34].

3 RESULTS AND DISCUSSION

3.1 Microstructure characterization and thermodynamic evaluation

The element distribution of the as-cast $CoCrNiSi_{0.3}$ and $CoCrNiSi_{0.15}$ MEAs are shown in Fig. 2, and we can clearly see the dendrite and Si segregation at the interdendritic region. The single-point quantitative component analysis results of these two regions are demonstrated in Table 1, and the content of Si at the interdendritic of $CoCrNiSi_{0.3}$ is about twice that at the interdendritic of $CoCrNiSi_{0.15}$. SDAS was also measured and organized in Table 1.

Through the microstructure characterization, we can observe that although the segregation of Si is significant, the as-cast $CoCrNiSi_{0.3}$ and $CoCrNiSi_{0.15}$ systems remain in a single phase. Thus, we considered CoCrNi the solvent and Si the solute to predict the pseudo-binary phase diagram for $CoCrNiSi_x$ MEAs in Thermo-Calc, as shown in Fig. 3(a).

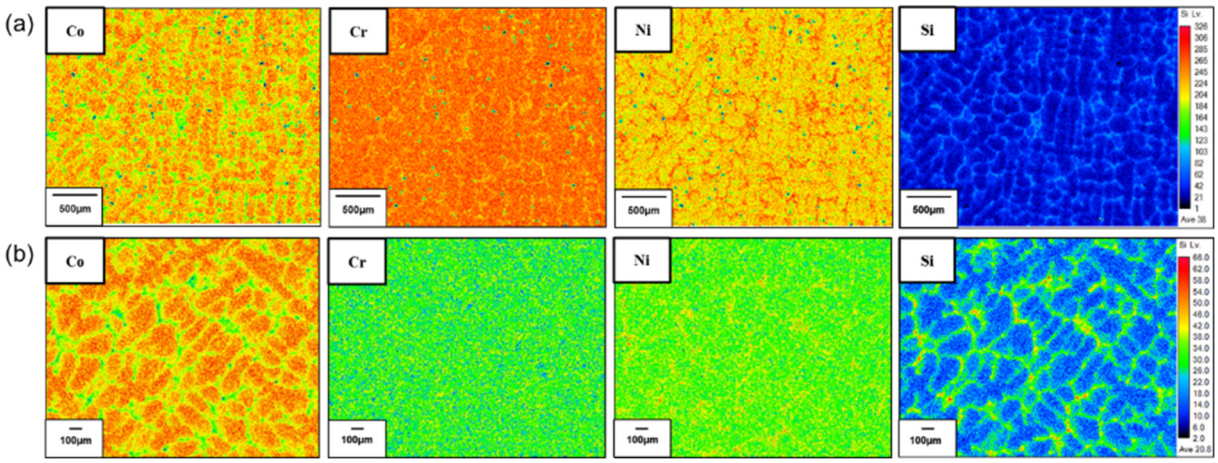

Figure 2. EPMA mapping results of (a) $CoCrNiSi_{0.3}$ and (b) $CoCrNiSi_{0.15}$

Table 1. The composition of dendritic/interdendritic region and SDAS of $CoCrNiSi_x$ MEAs

	Region	Co (at. %)	Cr (at. %)	Ni (at. %)	Si (at. %)	SDAS (μm)
$CoCrNiSi_{0.3}$	Dendritic	31.1	32.9	29.3	6.7	130 ± 30
	Interdendritic	20.2	28.7	33.0	18.1	
$CoCrNiSi_{0.15}$	Dendritic	33.9	31.6	31.1	3.4	110 ± 20
	Interdendritic	25.4	31.1	34.6	8.9	

In addition, due to the sluggish diffusion effect, the diffusion coefficient is quite low in HEAs/MEAs. Therefore, the Scheil solidification model was employed, which assumes no diffusion in solids, complete diffusion in liquids, and a local equilibrium maintained at the solid/liquid interface. The Scheil equation can be expressed as:

$$C_L = C_0(1 - f_S)^{(k-1)} \; ; \; C_S = kC_L \tag{7}$$

where C_L is the concentration in liquid, C_S is the concentration in solid, C_0 is the initial concentration, f_S is the solid fraction, and k is the partition coefficient equal to C_S/C_L. The Scheil solidification curves were plotted in Fig. 3(b). The solid fraction, density, Si composition in the solid, and the partition coefficient under the Scheil condition were demonstrated in Fig. 4. It is worth mentioning that the freezing range became much broader than that under equilibrium conditions. The composition of Si in the solid phase also gradually increased, as shown in Fig. 4(d), which explains why the Si atoms segregate in the interdendritic area. Additionally, Fig. 3(b) shows that the temperature at the last stage of solidification of $CoCrNiSi_{0.3}$ MEA is about 1166°C, which means some remaining liquid will solidify below the eutectic temperature (about 1176°C) in the pseudo-binary system.

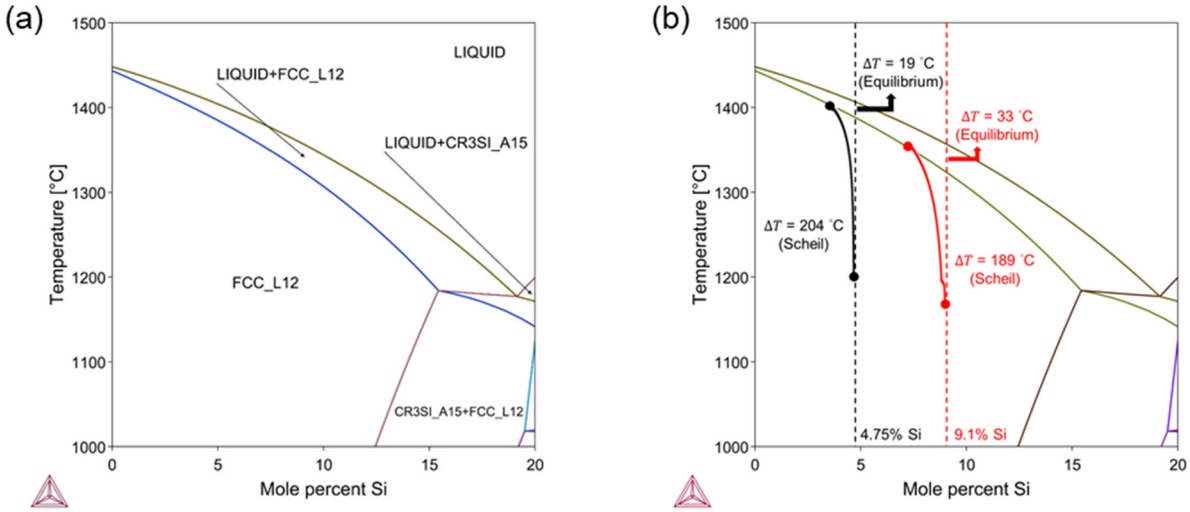

Figure 3. (a-b) Psuedo-binary phase diagram for $(CoCrNi)_{100-x}Si_x$, including the non-equilibrium solidification curve under the Scheil condition.

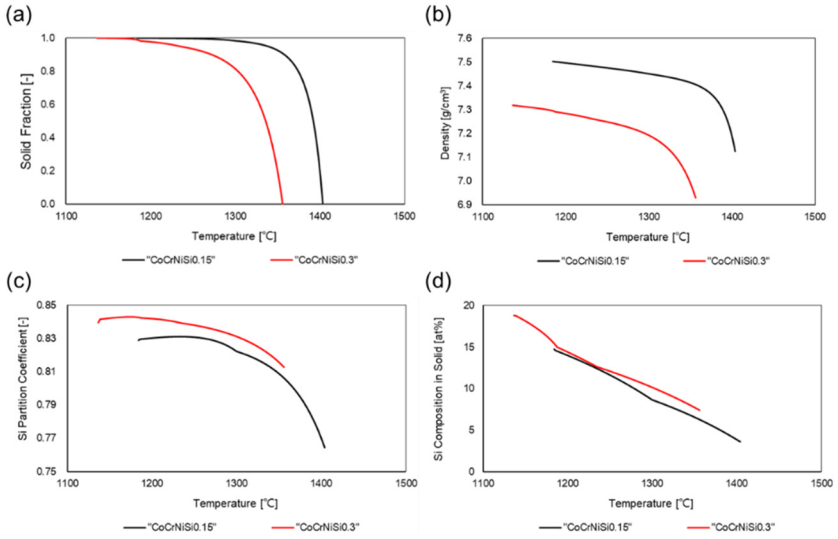

Figure 4. (a) Solid fraction, (b) density, (d) Si partition coefficient k, and (d) Si composition in solid evaluated by Thermo-Calc.

Thermo-Calc prediction and the experimental results of homogenization heat treatment were shown in Fig. 5. Noting that the distance in Fig. 5(a) represents the center of the secondary dendrite arm at 0 and the center of the interdendritic region at 70. The SDAS would be 140 μm in this setting, and the homogenization heat treatment should be completed in about 8 hours. However, the segregation of Si could be eliminated only after 48 hours of homogenization in the actual experiment (Fig. 5(b)). This difference indicated that diffusion coefficient evaluation and boundary conditions in the DICTRA model still need further modification.

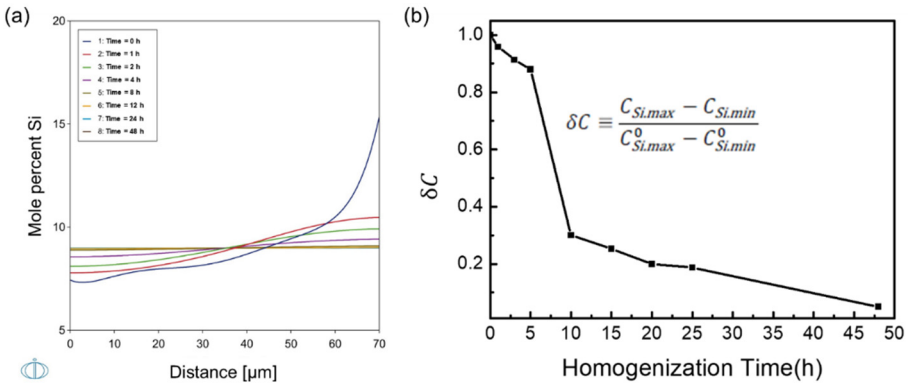

Figure 5. Homogenization heat treatment of (a) Thermo-Calc prediction using the DICTRA module and (b) the experimental results. The homogenization temperature was set at 1100°C both for simulation and experiment.

3.2 Macroscale heat transfer simulations

The results of the heat transfer simulation model are shown in Fig. 6. Due to the unequal Si content, the solidification behaviors of $CoCrNiSi_{0.3}$ and $CoCrNiSi_{0.15}$ MEAs are different, leading to the difference in the temperature, temperature gradient, cooling rate, and solid fraction during solidification. Scan line measurement was used to verify the rationality of these results, as shown in Fig. 7.

The higher temperature distribution before $t = 1500$ s $CoCrNiSi_{0.15}$ can be attributed to latent heat release due to earlier solidification. However, according to the simulation prediction, Fig. 7(b) shows the cooling rate of $CoCrNiSi_{0.15}$ is higher during solidification. The average cooling rate of $CoCrNiSi_{0.3}$ and $CoCrNiSi_{0.15}$ in the semi-solid region can be calculated as 0.18 K/s and 0.21 K/s, respectively, which explains why the SDAS of $CoCrNiSi_{0.15}$ is smaller than the SDAS of $CoCrNiSi_{0.3}$. Besides, some studies have detailed discussions on the relationship between SDAS and the cooling rate of HEAs or nickel-based superalloys and have summarized several empirical formulas [15-18]. If the simulation results are fitted into these formulas, there will be slight deviations, but considering the differences in materials, the predicted cooling rate is still within a reasonable range.

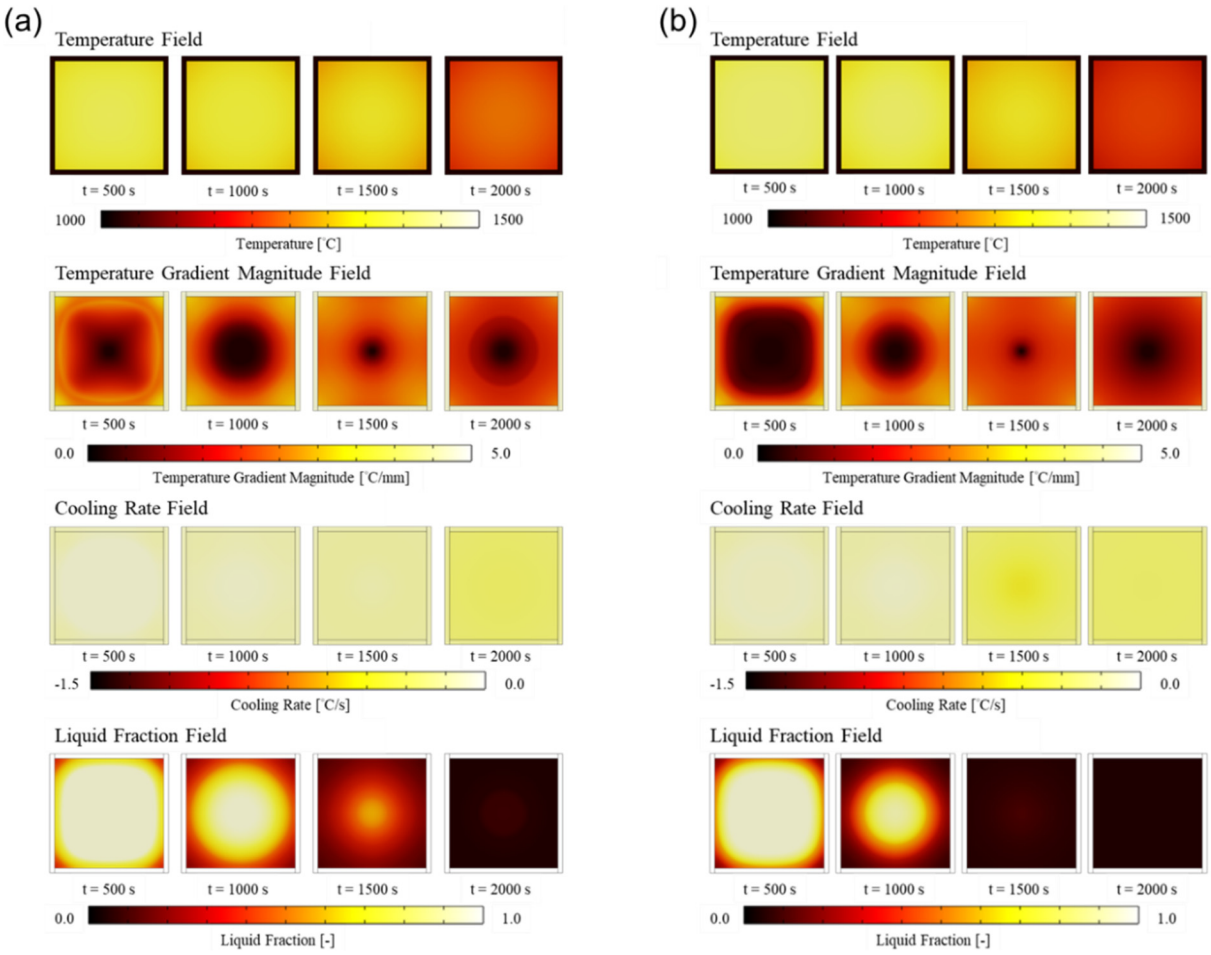

Figure 6. Temperature, temperature gradient, cooling rate, and solid fraction of (a) $CoCrNiSi_{0.3}$ and (b) $CoCrNiSi_{0.15}$ at different times during solidification

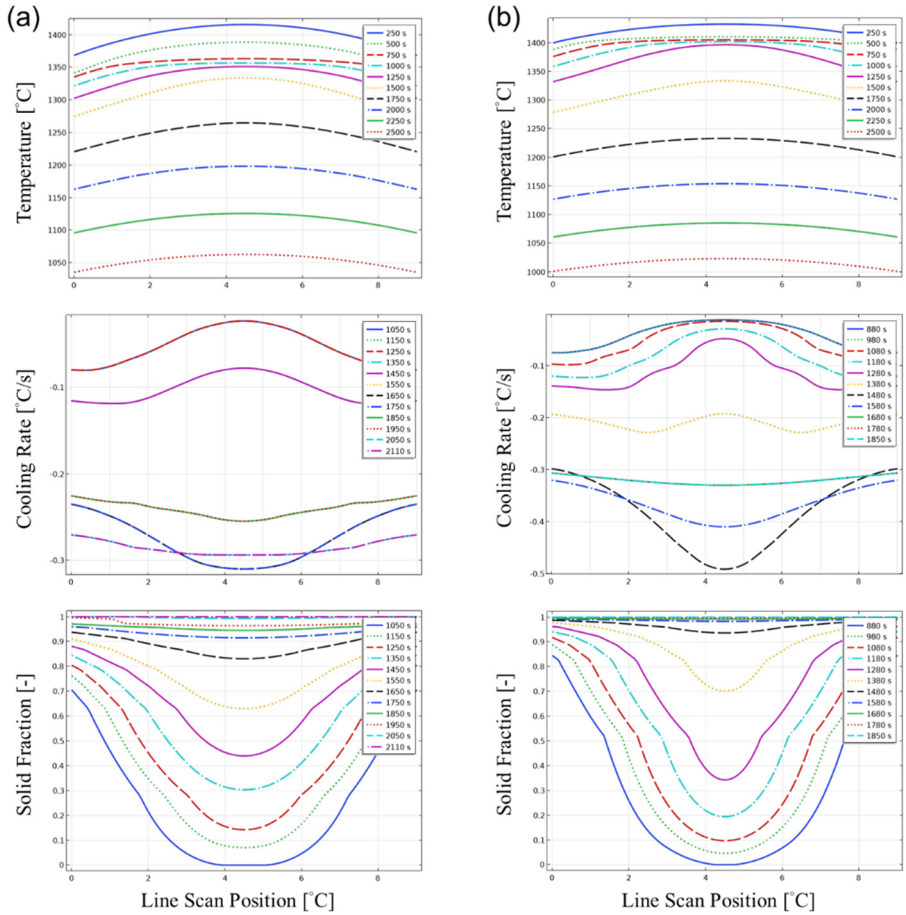

Figure 7. Temperature distribution at t = 250 ~ 2500 s in (a) $CoCrNiSi_{0.3}$ and (b) $CoCrNiSi_{0.15}$, as well as the cooling rate and solid fraction in the semi-solid region

3.3 Mesoscale phase field simulations

The MICRESS simulation results of microstructure evolution are demonstrated in Fig. 8. The solidification time range of $CoCrNiSi_{0.3}$ predicted by the phase field model is from $t = 1080$ s to $t = 2040$ s, which shows a good comparison with that predicted by COMSOL. As discussed before, $CoCrNiSi_{0.15}$ was predicted to solidify earlier than $CoCrNiSi_{0.3}$. However, the time range of solidification is only from $t = 990$ s to $t = 1520$ s. This is much shorter than the COMSOL prediction. In addition, the morphology and the size distribution of the second dendrite arms obtained from MICRESS looked quite uneven, and the SDAS was calculated to be about 300 μm for both MEAs. Besides, the Si concentration at the interdendritic of $CoCrNiSi_{0.3}$ is about twice that at the interdendritic of $CoCrNiSi_{0.15}$, but the content is about 20% less than the EPMA measurement (Table 1).

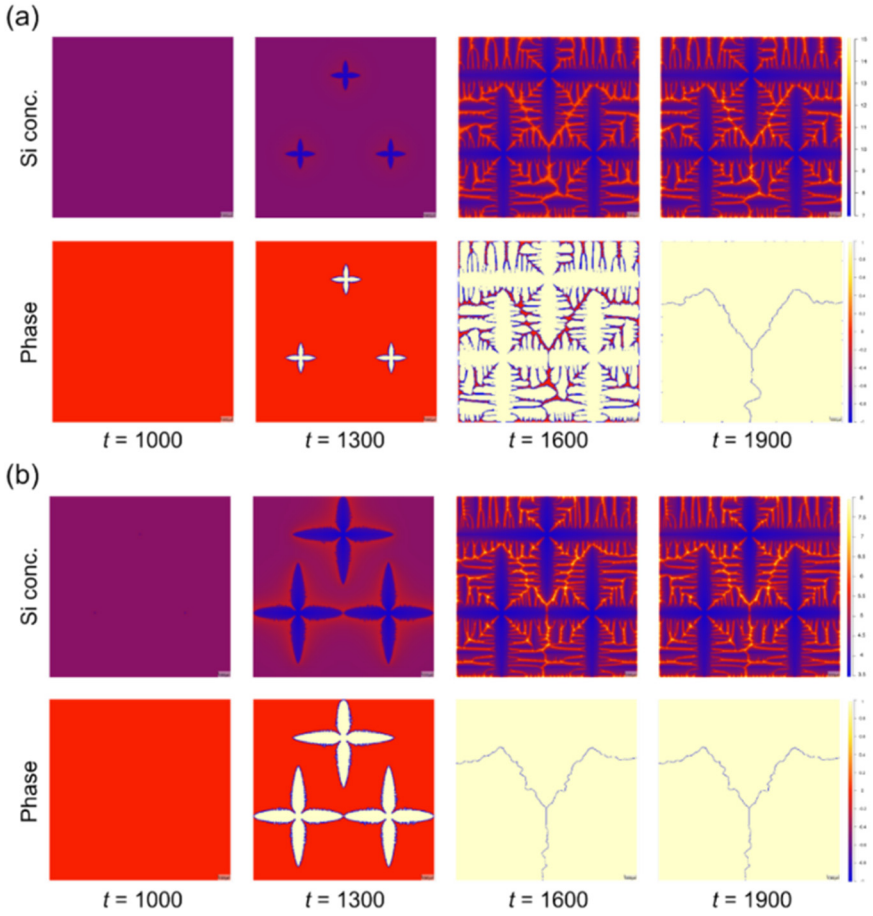

Figure 8. Si concentration field and phase field evolution of (a) $CoCrNiSi_{0.3}$ and (b) $CoCrNiSi_{0.15}$.

There are several possible reasons that could explain the differences between the current MICRESS phase field simulation results and the electron microscopy analysis findings. First, the geometry and the locations of the nuclei may need to be improved. The number of nuclei in a given region will affect the growth space and the concentration field during dendrite growth, further causing the difference in the morphology of the dendrites. Thus, only three nuclei may be too few for a 15mm x 15mm simulation area, leading to the dendrites growing too large. Second, the diffusion coefficients obtained from Thermo-Calc should be modified. We suspected that the diffusion coefficient of Si in $CoCrNiSi_x$ MEAs is too high, leading to excessive back diffusion. This results in less severe Si segregation at the interdendritic region compared to experimental observations and causes discrepancies in the SDAS. This situation may also explain why MICRESS predicted that the $CoCrNiSi_{0.15}$ MEA had completed solidification at $t = 1520$ s. Higher predicted diffusion rates of Si than the actual condition may also result in DICTRA predicting shorter homogenization times. The last thing that should be considered is the strength of anisotropy. According to the research by Kobayashi [30], changing the strength of anisotropy will cause a difference in dendrite morphology. In the future, using more precise combinations of thermodynamic and kinetic parameters is expected to simulate microstructures and element segregation patterns that more closely match experimental measurements.

4 CONCLUSIONS

A comprehensive approach combining experiments and multiscale simulation methods was developed to explore the correlation between the process parameters and the microstructure of industrial-grade $CoCrNiSi_x$ MEAs ingots. The CALPHAD method remarkably predicted the solidification behavior and Si segregation in the as-cast alloy while providing the necessary parameters for macroscopic heat transfer and mesoscopic phase field simulations. Using a finite element 2D heat transfer model, the temperature field, solid fraction field, and cooling rate field of $CoCrNiSi_x$ MEAs during the VIM with ceramic mold investment casting can be reasonably reproduced. The phase field model used the temperature variations from the macroscopic heat transfer simulations to simulate the microstructure evolution within $CoCrNiSi_x$ MEAs. However, the current mesoscopic phase-field simulation results do not entirely correlate with the experimental results. We hypothesize that three potential issues need to be modified: (i) the locations of the nuclei, (ii) the diffusion coefficients, and (iii) the interphase parameters such as anisotropy strength.

REFERENCES

[1] Z. Wu, H. Bei, F. Otto, G.M. Pharr, E.P. George, Recovery, recrystallization, grain growth and phase stability of a family of FCC-structured multi-component equiatomic solid solution alloys, *Intermetallics* **46** (2014) 131-140.

[2] H. Chang, T.W. Zhang, S.G. Ma, D. Zhao, R.L. Xiong, T. Wang, Z.Q. Li, Z.H. Wang, Novel Si-added CrCoNi medium entropy alloys achieving the breakthrough of strength-ductility trade-off, *Materials & Design* **197** (2021) 109202.

[3] R. Acharya, J.A. Sharon, A. Staroselsky, Prediction of microstructure in laser powder bed fusion process, *Acta Materialia* **124** (2017) 360-371.

[4] M.-H. Tsai, J.-W. Yeh, High-Entropy Alloys: A Critical Review, *Materials Research Letters* **2**(3) (2014) 107-123.

[5] J.W. Yeh, S.K. Chen, S.J. Lin, J.Y. Gan, T.S. Chin, T.T. Shun, C.H. Tsau, S.Y. Chang, Nanostructured High-Entropy Alloys with Multiple Principal Elements: Novel Alloy Design Concepts and Outcomes, *Advanced Engineering Materials* **6**(5) (2004) 299-303.

[6] J.W. Yeh, Recent progress in high entropy alloys, *Annales de Chimie - Science des Matériaux* **31**(6) (2006) 633-648.

[7] B. Gludovatz, A. Hohenwarter, K.V.S. Thurston, H. Bei, Z. Wu, E.P. George, R.O. Ritchie, Exceptional damage-tolerance of a medium-entropy alloy CrCoNi at cryogenic temperatures, *Nature Communications* **7**(1) (2016) 10602.

[8] D. Lee, H.-U. Jeong, K.-H. Lee, J.B. Jeon, N. Park, Precipitation and grain-boundary strengthening of Al-added CoCrNi medium-entropy alloys, *Materials Letters* **250** (2019) 127-130.

[9] H. Yi, M. Bi, K. Yang, B. Zhang, Significant Improvement the Mechanical Properties of CoCrNi Alloy by Tailoring a Dual FCC-Phase Structure, *Materials* **13**(21) (2020) 4909.

[10] W. Lu, X. Luo, Y. Yang, J. Zhang, B. Huang, Effects of Al addition on structural evolution and mechanical properties of the CrCoNi medium-entropy alloy, *Materials Chemistry and Physics* **238** (2019) 121841.

[11] G.W. Hu, L.C. Zeng, H. Du, X.W. Liu, Y. Wu, P. Gong, Z.T. Fan, Q. Hu, E.P. George, Tailoring grain growth and solid solution strengthening of single-phase CrCoNi medium-entropy alloys by solute selection, *Journal of Materials Science & Technology* **54** (2020) 196-205.

[12] W. Kurz, D.J. Fisher, Dendrite growth at the limit of stability: tip radius and spacing, *Acta Metallurgica* **29**(1) (1981) 11-20.

[13] M.M. Franke, R.M. Hilbinger, C.H. Konrad, U. Glatzel, R.F. Singer, Numerical Determination of Secondary Dendrite Arm Spacing for IN738LC Investment Castings, *Metallurgical and Materials*

Transactions A **42**(7) (2011) 1847-1853.
[14] J.A. Dantzig, M. Rappaz, *Solidification*, EPFL Press, London, 2009.
[15] Y. Zhang, B. Huang, J. Li, Microstructural Evolution with a Wide Range of Solidification Cooling Rates in a Ni-Based Superalloy, *Metallurgical and Materials Transactions A* **44**(4) (2013) 1641-1644.
[16] V. Kavoosi, S.M. Abbasi, S.M.G. Mirsaed, M. Mostafaei, Influence of cooling rate on the solidification behavior and microstructure of IN738LC superalloy, *Journal of Alloys and Compounds* **680** (2016) 291-300.
[17] J. Nawrocki, M. Motyka, D. Szeliga, W. Ziaja, R. Cygan, J. Sieniawski, Effect of cooling rate on macro- and microstructure of thin-walled nickel superalloy precision castings, *Journal of Manufacturing Processes* **49** (2020) 153-161.
[18] H. Zheng, Q. Xu, R. Chen, G. Qin, X. Li, Y. Su, J. Guo, H. Fu, Microstructure evolution and mechanical property of directionally solidified CoCrFeMnNi high entropy alloy, *Intermetallics* **119** (2020) 106723.
[19] X. Zhang, J. Zhao, H. Jiang, M. Zhu, A three-dimensional cellular automaton model for dendritic growth in multi-component alloys, *Acta Materialia* **60**(5) (2012) 2249-2257.
[20] M.A. Easton, D.H. StJohn, A model of grain refinement incorporating alloy constitution and potency of heterogeneous nucleant particles, *Acta Materialia* **49**(10) (2001) 1867-1878.
[21] X.W. Liu, G. Laplanche, A. Kostka, S.G. Fries, J. Pfetzing-Micklich, G. Liu, E.P. George, Columnar to equiaxed transition and grain refinement of cast CrCoNi medium-entropy alloy by microalloying with titanium and carbon, *Journal of Alloys and Compounds* **775** (2019) 1068-1076.
[22] X.W. Liu, L. Liu, G. Liu, X.X. Wu, D.H. Lu, J.Q. Yao, W.M. Jiang, Z.T. Fan, W.B. Zhang, The Role of Carbon in Grain Refinement of Cast CrFeCoNi High-Entropy Alloys, *Metallurgical and Materials Transactions* A **49**(6) (2018) 2151-2160.
[23] R.W. Hamilton, D. See, S. Butler, P.D. Lee, Multiscale modeling for the prediction of casting defects in investment cast aluminum alloys, *Materials Science and Engineering: A* **343**(1) (2003) 290-300.
[24] A. Sabau, Numerical simulation of the investment casting process, *Transactions of American Foundry Society* **113** (2005) 407-417.
[25] A. Reikher, K.M. Pillai, A fast simulation of transient metal flow and solidification in a narrow channel. Part II. Model validation and parametric study, *International Journal of Heat and Mass Transfer* **60** (2013) 806-815.
[26] M.M. Behera, S. Pattnaik, M.K. Sutar, Thermo-mechanical analysis of investment casting ceramic shell: A case study, *Measurement* **147** (2019) 106805.
[27] I. Loginova, G. Amberg, J. Ågren, Phase-field simulations of non-isothermal binary alloy solidification, *Acta Materialia* **49**(4) (2001) 573-581.
[28] R. Kobayashi, Modeling and numerical simulations of dendritic crystal growth, *Physica D: Nonlinear Phenomena* 63(3) (1993) 410-423.
[29] J.L. Li, Z. Li, Q. Wang, C. Dong, P.K. Liaw, Phase-field simulation of coherent BCC/B2 microstructures in high entropy alloys, *Acta Materialia* 197 (2020) 10-19.
[30] R. Rettig, N.C. Ritter, F. Müller, M.M. Franke, R.F. Singer, Optimization of the Homogenization Heat Treatment of Nickel-Based Superalloys Based on Phase-Field Simulations: Numerical Methods and Experimental Validation, *Metallurgical and Materials Transactions A* 46(12) (2015) 5842-5855.
[31] A. Bejan, A.D. Kraus, *Heat transfer handbook*, John Wiley & Sons, 2003.
[32] J. Eiken, B. Böttger, I. Steinbach, Multiphase-field approach for multicomponent alloys with extrapolation scheme for numerical application, *Physical Review E* 73(6) (2006) 066122.
[33] B. Böttger, J. Eiken, M. Apel, Phase-field simulation of microstructure formation in technical castings – A self-consistent homoenthalpic approach to the micro–macro problem, *Journal of Computational Physics* 228(18) (2009) 6784-6795.
[34] B. Böttger, J. Eiken, M. Apel, Multi-ternary extrapolation scheme for efficient coupling of thermodynamic data to a multi-phase-field model, *Computational Materials Science* 108 (2015) 283-292.